DIFFERENTIAL POLARIZATION REFLECTIVITY AT 1.574 μm EYE-SAFE BACKSCATTER LIDAR

J. Fochesatto, K. Sassen, R. L. Collins

Geophysical Institute, University of Alaska Fairbanks. Fairbanks, AK 99775 (foch@gi.alaska.edu)

ABSTRACT

A preliminary analysis of differential polarization reflectivity lidar signals is reported using a novel Eye-Safe Backscatter Lidar with polarization diverse at 1.574 μm. The instrument is based on a previously designed, single-channel Compact Eye-Safe Backscatter Lidar CESBL[1] assembled in a compact optical bench instrumentation platform. The instrument was upgraded for polarization selectivity in the laser emission and linear polarization discrimination in the receiver unit. The instrument has computer controlled polarization selectivity in the laser emission and is able to perform sequential measurements at different polarization modes including both linear and circular polarization. The lidar design focuses on high accuracy, better than 60 dB, in polarization emission and polarization discrimination accuracy over 50 dB. These features allow depolarization ratios and polarimetric parameters retrieval to of ~0.1%.

Applications for this instrument includes aerosol physical processes in the lower troposphere under a variety of conditions (i.e. ice fog, arctic haze, complex aerosol, aerosol-cloud interaction and cirrus clouds studies), and meteorological and environmental issues in the Arctic (i.e. forest fire aerosol products, boundary layer dynamic in extreme Arctic conditions).

INTRODUCTION

Aerosols in the troposphere have broad impact ranging from human health effects to global climate change. Scattering and absorption characteristics of aerosols have a variety of implications in the troposphere (i.e. seeding tropospheric clouds and, formation of haze and fog, thereby redistributing the incoming solar flux and the infrared terrestrial emission, and altering the radiation balance of the earth system. Tropospheric aerosol research deserves special attention because of its multifunctional role in the aerosol-atmosphere interaction, driving various feedback mechanisms. Particular aerosols processes include: nucleation process in the boundary layer (BL); downward mixing of transported aerosols that may be responsible for episodic high surface concentration of fine particulate matter and ozone; dense aerosols layers during smoke episodes; formation of ice fog and tropospheric icy clouds by heterogeneous freezing in polar environments, variations in the microphysical properties of BL aerosols due to BL cycling.

Aerosols in the Arctic context are a target for geophysical study because of the long-term isolation between the atmosphere in the Earth's different climatic regions [9]. The overall role of aerosol interactions is very difficult to quantify and it is widely recognized as a leading cause of uncertainty in current climate change predictions [8].

Improving our understanding of the aerosol interaction process requires precise identification of different aerosols properties. In particular chemical speciation is a crucial step towards a full description of the aerosol-atmosphere interaction. Polarization lidars with scanning capabilities can identify and distinguish cloud and aerosol phase state (liquid from ice), aerosol properties (absorbing from pure scattering aerosols), spherical aerosols (water droplets) from non-spherical aerosols, and ice crystal orientation [6, 7]. Moreover, lidar system that can manipulate the polarization emission (hare after named "diversity") offers the possibility of further exploring the total scattering matrix of aerosol and clouds layers making possible new physical quantities (i.e. diverse depolarization ratios), improving physical processes description and quantitative magnitude retrievals (i.e. ice/water fraction) under conditions of multiple scattering).

THEORY OF POLARIZATION DIVERSITY LIDARS

The complete polarization state of a light beam coherent or non-coherent can be represented by measurable quantities using the Stokes vector components S = {I, Q, U, V} [2]. The general form of a polarized beam in the Stokes parameters representation is given in Eq (1); where the subscript *l* and *r* refers to the electric field parallel and perpendicular respectively to the scattering plane and brackets denote time averages. The four elements of the Stokes vector are specified as: the total beam intensity (I), the dominant l-polarization over r-polarization state in the beam (Q), same for +45 over -45 (U) and right circular polarization over left circular polarization (V).

$$\begin{aligned} I &= \left\langle E_l \cdot E_l^* + E_r \cdot E_r^* \right\rangle \\ Q &= \left\langle E_l \cdot E_l^* - E_r \cdot E_r^* \right\rangle \\ U &= \left\langle E_l \cdot E_r^* + E_r \cdot E_l^* \right\rangle \\ V &= i\left\langle E_l \cdot E_r^* - E_r \cdot E_l^* \right\rangle \end{aligned} \quad (1)$$

The Stokes vector can thus describe the incident beam and the scattered beam at a given layer in the atmosphere and their relationship is given be the sixteen-element of the Mueller matrix. The scattering matrix components S_{ij} contain information about the size distribution, shape and refractive index of the scatters. The elements of this scattering matrix are dependent of: scattering angle, wavelength and the specific microphysical state and optical properties of the particular atmospheric layer.

Scattering matrix simplifications are generally considered in well-known cases, but potentially the 16 elements may be significant for certain environments involving non-randomly oriented non-spherical particles. For the case of light scattered by randomly oriented aerosols the scattering matrix simplifies into 10 unknown coefficients for each scattering angle [3]. In this case the randomly oriented distribution of scatterers supposes that each particle and its mirrored one scatter light at the same time. For an anisotropic distribution of aerosols, the scattering matrix evaluated in the backscattered direction (180^o) can be simplified as indicated in [4]. For spherical particles, only four independent matrix elements are needed to describe the interaction with arbitrarily polarized light, because spherically symmetrical particles (e.g., cloud droplets) do not produce any change in the backscattered polarization state in single scattering [5]. An anisotropic distribution of particles may yield $S_{14} \neq 0$, but an isotropic distribution, perhaps the usual case representing randomly-oriented non-spherical particles in the atmosphere, has $S_{14}=0$.

It is also well known that particles are not always present in the atmosphere with random orientation in fact they can be slightly oriented; they can also be slightly spherical, and in other cases multiple scattering may complicate severely the solid/liquid phase fraction determination when a reduced type of Mueller matrix is considered. For those cases a lidar with diverse polarization bring new observable quantities related to the scattering coefficients S_{ij} that permits a full characterization of the scattering process.

The application of the polarization diversity theory relies on the measurement of different ratios (polarization factors) at different angular positions related to the combination of scattering matrix coefficient S_{ij}. In order to obtain this measurement together with the corresponding calibration, it is necessary to induce different polarization states in the laser emission $\{I_I, Q_I, U_I, V_I\}$ and analyze a set of different polarization states of the backscattered field at the lidar detection level $\{I_S, Q_S, U_S, V_S\}$.

POLARIZATION DIVERSITY EMISSION

In order to implement the polarization emission control it is necessary to initially define the linear polarization of the emission with very high precision. In this case a Brewster angle polarizer was chosen to define the initial polarization state of the laser beam due to their high polarization selectivity. Brewster angle polarizer's are made by two calcite prisms assembled with an air space. The polarizer transmits extraordinary polarization whereas each of the four faces are placed at Brewster angle making transmission lost at extraordinary polarization less than 2% with ~ 60 dB extinction for ordinary polarization. The polarizer Brewster angle was specified at approximate $\lambda_{laser}/2$ of flatness with surface crystal AR-coating to maximize the optical throughput of the extraordinary beam.

The polarization state is manipulated with a photoelastic modulator (PEM). The PEM is arranged with an initial positive angle φ referred to the initial laser polarization state (whereas [+] means angles clockwise looking in the direction of the propagation of the laser beam). The optical modulator produces refractive index variation over a crystal driven by a piezoelectric modulator with a frequency of 42 kHz with +/- 1Hz of uncertainty. Based on the very precise PEM excitation frequency, with an accuracy of less than 0.005%, a phase-locked loop circuit produces a synchronous signal at different phase retardation that can be selected by the operator. This signal hereafter named "retardation level" indicates the instantaneous state of the PEM phase after the corresponding optoelectronic calibration. Eq. 2 shows the polarization beam transformation after passing through the PEM modulator the total optical phase rotation is (ψ+φ).The PEM was assembled in a precision goniometric platform to allow opto-mechanical adjustments and polarization calibration.

$$\begin{bmatrix} I_O \\ Q_O \\ U_O \\ V_O \end{bmatrix} = \begin{bmatrix} 1 & 0 & 0 & 0 \\ 0 & \cos(2\cdot(\psi+\varphi)) & -\sin(2\cdot(\psi+\varphi)) & 0 \\ 0 & \sin(2\cdot(\psi+\varphi)) & \cos(2\cdot(\psi+\varphi)) & 0 \\ 0 & 0 & 0 & 1 \end{bmatrix} \times \begin{bmatrix} I_I \\ Q_I \\ U_I \\ V_I \end{bmatrix} \quad \text{Eq. 2}$$

.

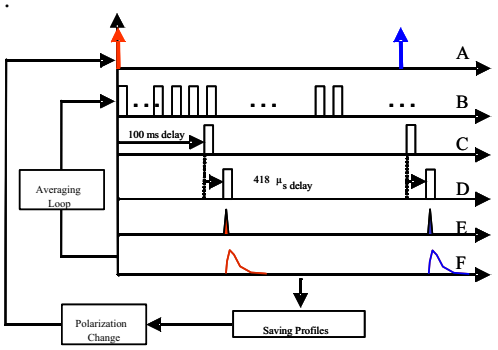

Fig.1. ESPDL timing diagram for polarization selectivity. A) is the computer selection retardation level applied to the PEM modulator. B) is the PEM synchronization pulses 42 +/- 1 Hz. C) Flash Lamp laser trigger at 10 Hz; D) Laser Q-switch pulses 300 μsec width; E) Laser optical emission and F) is the lidar signal

In this laboratory calibration two levels of PEM control signal were used to induce two linear polarization states in the laser emission. To produce the linear polarization state {1,1,0,0} the phase angle to be induced has to be -π/4 and to generate {1,-1,0,0} the corresponding phase angle has to be π/4 . Fig. 1 shows the electronic timing diagram for the computer controlled polarization selectivity

POLARIZATION RECEIVER

The receiver telescope is a commercial Cassegrain F/10–2 m focal length. The optical throughput is less than 40 % at the laser wavelength. A custom Dall-Kirkham type telescope (F/3-900 mm with zero focal drift and very low coefficient of thermal expansion) [1] was designed and constructed. The polarization receiver was implemented in a mechanical assembly containing the interferential filter, a half-wave plate and the polarizer splitter. The mechanical assembly containing the polarization beam splitter, the focusing optics and detectors units are able to rotate around the optical axis. This opto-mechanical design facilitates the optical alignment, the electronic calibration and maximizes the polarization matching between the laser emission and the receiver subsystem. A Glan Thompson polarizer beam splitter is used to separate the two orthogonal polarization components. This polarizer is made of two cemented prisms of calcite. For an input beam at normal incidence to the polarizer input face, the polarizer split the beam into two orthogonally polarized output beams that exits the crystal at normal incidence to their respective output faces having a separation angle of 45 degree independent of the wavelength. The cross-talk extinction ratio is better than 50 dB.

DIFFERENTIAL POLARIZATION REFLECTIVITY ANALYSIS

An analysis of the differential polarization reflectivity based on observations where the laser emission was setup to sequentially transmit in two linear polarization states (i.e. {1,1,0,0} and {1,-1,0,0}) and the receiver was assembled in a single channel without polarization discrimination. The backscattered beam can be expressed as in Eq.3.

$$\begin{bmatrix} I_S \\ Q_S \\ U_S \\ V_S \end{bmatrix} = \begin{bmatrix} S_{11} & S_{12} & 0 & 0 \\ S_{21} & S_{22} & 0 & 0 \\ 0 & 0 & S_{33} & S_{34} \\ 0 & 0 & S_{43} & S_{44} \end{bmatrix} \times \left\{ \begin{bmatrix} 1 \\ 1 \\ 0 \\ 0 \end{bmatrix} \wedge \begin{bmatrix} 1 \\ -1 \\ 0 \\ 0 \end{bmatrix} \right\} \quad \text{Eq 3.}$$

The backscatter power (hereafter named P_V for the case of {1,1,0,0} emission and P_H for the case of {1,-1,0,0}) is expressed in terms of the S_{ij} coefficients. The two differential reflectivity observables can be related to the S_{ij} coefficients as in Eq.4.

$$Z_{DRI} = \frac{P_V - P_H}{2} = S_{22} + S_{12}$$
$$Z_{DRII} = \frac{P_V + P_H}{2} = S_{11} + S_{12} \quad \text{Eq. 4}$$

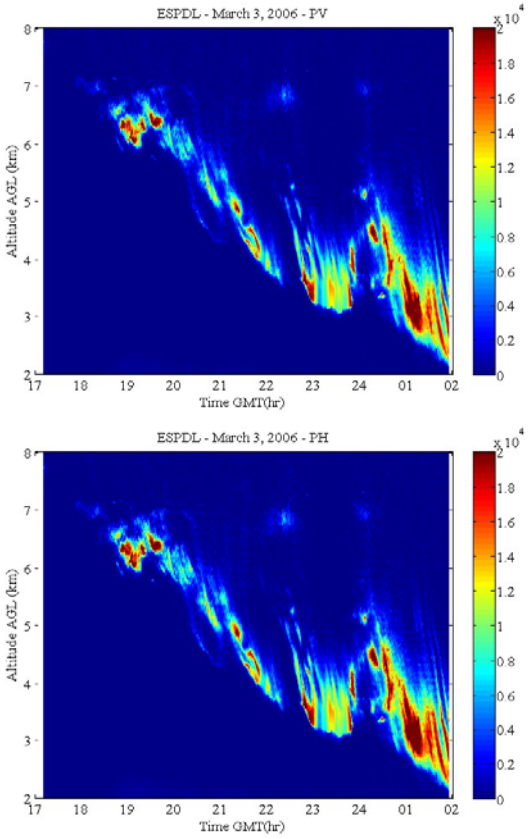

Fig.2. Eye-Safe Lidar backscatter power ($P.Z^2$) vertical pointing during March 3, 2006 at the Geophysical Institute in Fairbanks, AK. Upper panel represents the vertical polarization reflectivity (P_V). Lower panel is the time series for the alternate linear polarization emission made in Horizontal (P_H).

A cirrus clouds is depicted in Fig.2 during morning hours. It is observed to subside from 7.0 km down to 2.5 km AGL. Aerosols (possibly Asian dust) are present in the lowest troposphere below 2 km, but not showing here.

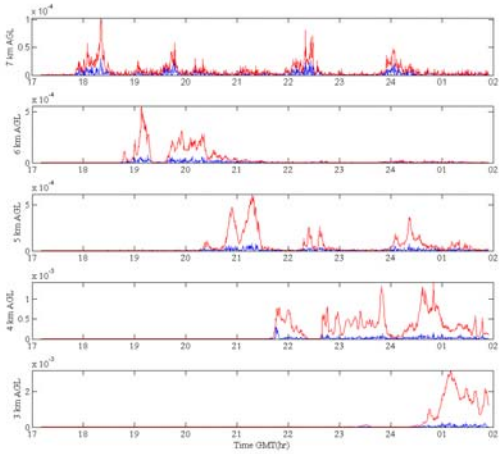

Fig.3 Differential polarization reflectivity ZDRI (blue color trace) and ZDRII (red trace) at different AGL altitudes 7, 6, 5, 4, 3 km.

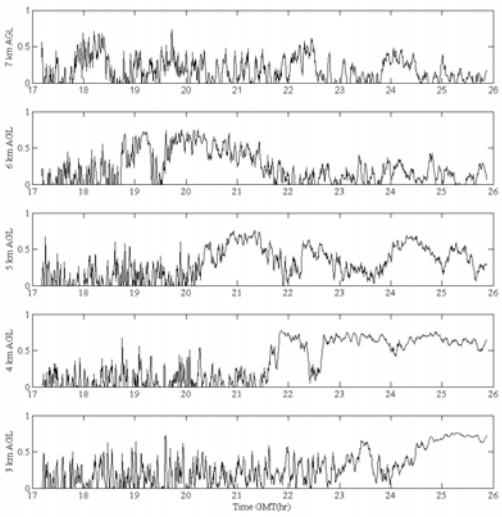

Fig.4 Linear polarization factor at different altitudes based on Differential polarization reflectivity ZDRI and ZDRII at 7 km, 6 km, 5 km, 4 km, 3 km.

Temporal series in Fig. 3 shows the independent variation of S_{11} and S_{22}. This differs from linear co-polar analysis where these two coefficients are related by the depolarization factor. A Stokes equivalent polarization factor can be calculated based on these two differential reflectivity observables Eq 5.

$$\delta^{*} = \frac{Z_{DRII} - Z_{DRI}}{Z_{DRII} + Z_{DRI}} \quad \text{Eq.5}$$

Fig. 4 shows the temporal evolution of the δ* factor at different altitudes the background level of this factor was calculated above 7 km (region free of clouds and aerosols) and subtracted in Fig. 4.

SUMMARY

Both Fig.2 and Fig. 3 reveals significant differences and evolution in the backscatter power and in the differential reflectivity. The differential reflectivity of the cirrus cloud at 7 km has variations that are almost three times greater than the noise variations. This suggests that the cloud undergoes significant evolution while the cloud is subsiding. In particular these differences are seen on the cirrus cloud base indicating some preferential particles orientation relative to the cirrus cloud top.

The depolarization factors in Fig.4 show morphological changes and trends associated with the presence of both clouds and aerosols in a subsiding air mass.

A new eyesafe lidar instrument is under development at the Geophysical Institute-University of Alaska Fairbanks. The lidar has novel capabilities that allows complete polarization control in the laser emission. The receiver subsystem is currently being upgraded to include the receiver features described in this article.

Based on initial observations, differential reflectivity analyses (and their similarities or differences with classical linear depolarization) are very promising elements for future analysis and characterization of clouds, aerosols and their thermodynamic environment.

ACKNOWLEDGEMENTS

The project was funded by: University Partnering for Operational support program; supported by the United States Air Force under contract number N00024-03-D-6606 and performed in connection with contract DAAD19-02-D-0003 with the U.S. Army Research Laboratory and by NSF-MASINT – Measures and Signatures Intelligence IRS 92-6000147.

REFERENCES

[1] Fochesatto J., Collins R., Yue J., Cahill C., Sassen K. (2005). Proc. of SPIE Vol. 5887. doi: 10.1117/12.620970.

[2] Bohren, CF and DR Huffman, (1983). *Absorption and Scattering of Light by Small Particles*, John Wiley & Sons.

[3] Hovenier J., H. C. van de Hulst and C.V.M. van der Mee. (1986). *Astron. Astrophys*. 157, 301-310.

[4] Perrin, F. (1942). *J. Chem. Phys.*, *10*, 415-427.

[5] Sassen, K and KN Liou. (1979). *J. Atmos. Sci*., *36*, 838-851.

[6] Sassen, K, (1991). *Bull. Amer. Meteor. Soc., 72*, 1848-1866.

[7] Sassen, K. (2005b). *Polarization in Lidar*, in "Lidar", Springer Press, C. Weitkamp, Ed., 19-42.

[8] IPCC (2001). National Academy of Science [http://books.nap.edu/books/0309075742/html/].

[9] IGAC (2004). International Global Atmospheric Chemistry IGAC (http://www.igac.noaa.gov/)